Developmental Biology 413 (2016) 160–172

Contents lists available at ScienceDirect

Developmental Biology

journal homepage: www.elsevier.com/locate/developmentalbiology

Osterix/Sp7 limits cranial bone initiation sites and is required for formation of sutures

Erika Kague [a,*,1], Paula Roy [a,2], Garrett Asselin [b], Gui Hu [a], Jacqueline Simonet [a], Alexandra Stanley [c], Craig Albertson [b], Shannon Fisher [a,*,3]

[a] Department of Cell and Developmental Biology, Perelman School of Medicine at the University of Pennsylvania, Philadelphia, PA, USA
[b] Department of Biology, University of Massachusetts, Amherst, MA, USA
[c] Cell and Molecular Biology Graduate Program, Perelman School of Medicine at the University of Pennsylvania, Philadelphia, PA, USA

ARTICLE INFO

Article history:
Received 10 March 2016
Accepted 11 March 2016
Available online 16 March 2016

Keywords:
Osterix/Sp7
Craniofacial skeleton
Sutures
Osteogenesis
Zebrafish mutant

ABSTRACT

During growth, individual skull bones overlap at sutures, where osteoblast differentiation and bone deposition occur. Mutations causing skull malformations have revealed some required genes, but many aspects of suture regulation remain poorly understood. We describe a zebrafish mutation in *osterix/sp7*, which causes a generalized delay in osteoblast maturation. While most of the skeleton is patterned normally, mutants have specific defects in the anterior skull and upper jaw, and the top of the skull comprises a random mosaic of bones derived from individual initiation sites. Osteoblasts at the edges of the bones are highly proliferative and fail to differentiate, consistent with global changes in gene expression. We propose that signals from the bone itself are required for orderly recruitment of precursor cells and growth along the edges. The delay in bone maturation caused by loss of Sp7 leads to unregulated bone formation, revealing a new mechanism for patterning the skull and sutures.

1. Introduction

During growth of the vertebrate brain, it is encased and protected by the skull. The bones of the skull vault are joined by fibrous sutures during growth, which provide mechanical support while still allowing expansion of the brain and, in mammals, allowing for deformation of the skull during birth. The sutures also serve as sites of osteogenesis, where new bone is deposited primarily along the edges of the bones, at the osteogenic fronts. This specific spatial arrangement is highly conserved among vertebrates, including zebrafish (Laue et al., 2011; Quarto and Longaker, 2005). In many organisms, including humans, the calvarial bones fuse later in life, obliterating the sutures, although they largely remain patent in other species, including mice and zebrafish.

The sutures are sensitive to small changes in the process of osteoblast differentiation. For example, mutations thought to promote osteoblast differentiation, such as activating mutations in the FGF receptors, cause premature suture fusion, or craniosynostosis (Morriss-Kay and Wilkie, 2005). Conversely, haploinsufficiency for *RUNX2*, leading to delayed osteoblast differentiation, is associated with slower skull bone growth and delayed suture closure (Lee et al., 1997). The evaluation of these and other mutations has led to a model in which undifferentiated mesenchymal stem cells within the sutures are recruited to form early osteoblasts at the edges of the bones; as the bones grow, the osteoblasts become more differentiated as they are pushed farther away from the sutures by new bone deposition (Morriss-Kay and Wilkie, 2005). The spatial organization of the sutures makes them an excellent paradigm to examine the process of osteoblast differentiation.

However, many aspects of suture regulation remain poorly understood, for example the signals that recruit mesenchymal cells to enter the osteoblast pool. There are also disturbances in skull formation that cannot be explained by this simple model. One example is the formation of Wormian bones, ectopic skull bones entirely surrounded by sutures (Bellary et al., 2013). Small Wormian bones are a common finding in otherwise normal human skulls (Marti et al., 2013), but larger Wormian bones occur with greater frequency in association with mechanical deformation of the skull during growth (O'Loughlin, 2004), as well as in genetic diseases causing both delayed suture closure (Cremin et al., 1982;

* Correspondence to: Department of Genetics and Evolutionary Biology São Paulo University, Rua do Matão 277, São Paulo, SP 05508-090, Brazil and Department of Pharmacology and Experimental Therapeutics, Boston University School of Medicine, 72 East Concord St., Boston, MA 02118, USA.
E-mail addresses: ekague@ib.usp.br (E. Kague), shanfish@bu.edu (S. Fisher).
[1] Current address: Department of Genetics and Evolutionary Biology, University of São Paulo, SP, Brazil.
[2] Current address: Department of Ecology and Evolutionary Biology, University of Kansas, Lawrence, KS, USA.
[3] Current address: Department of Pharmacology and Experimental Therapeutics, Boston University School of Medicine, Boston, MA, USA.

http://dx.doi.org/10.1016/j.ydbio.2016.03.011

Otto et al., 2002)and craniosynostosis (Sanchez-Lara et al., 2007). Simultaneous inactivation of the *Msx1* and *Msx2* genes in mouse leads to prominent ectopic skull bone formation, suggesting that repression of BMP signaling in non–osteogenic regions normally prevents their formation (Roybal et al., 2010). However, because of the association of Wormian bones with a wide variety of skull malformations, and the relative lack of animal models, little is understood about their mechanism of formation.

Osterix/Sp7 is a zinc finger transcription factor required for proper osteoblast differentiation during skeletal development in the mouse (Nakashima et al., 2002). Its specific expression in osteoblasts is conserved across species (DeLaurier et al., 2010; Li et al., 2009; Miura et al., 2008; Renn and Winkler, 2009), although the gene has not been mutated in any other model organism. Conditional inactivation of the gene postnatally in mice supports a continued role for Sp7 in bone homeostasis (Baek et al., 2010), and in humans genome wide association studies (GWASs) have implicated *SP7* in variation in bone mineral density (Rivadeneira et al., 2009; Styrkarsdottir et al., 2009; Timpson et al., 2009; Zhao et al., 2011). Depletion of *sp7* with antisense morpholinos in medaka larvae does not completely inhibit bone formation, but causes a general delay in bone growth, with a concomitant suppression of mature osteoblast marker expression (Renn and Winkler, 2014). Recently a human patient homozygous for a mutation in *SP7* was described (Lapunzina et al., 2010). Consistent with the roles ascribed to the gene through GWAS and in mouse and medaka, the patient had severe defects in bone growth and mineralization and suffered frequent fractures. He also displayed craniofacial malformations and developed Wormian bones, suggesting a link between the general phenotypes in bone differentiation and the specific patterning of the skull bones.

We describe a zebrafish mutation in *sp7*, which causes defects in bone growth and mineralization, although the early skeleton of mutants is normally patterned and the fish are viable. This has allowed us to examine skull development, which occurs in juvenile fish during the period of 3–6 weeks post fertilization (wpf). Importantly, the accessibility of zebrafish throughout this critical period allows us to observe the dynamics of skull formation in live fish. We find that *sp7* mutants have multiple, irregular skull bones, with virtually no normally patterned sutures or skull bones. This is correlated at the cellular level with delayed differentiation and excessive proliferation of early osteoblasts, and increased BMP signaling in and surrounding the sutures. Our findings suggest that signaling from differentiating bone controls recruitment of new cells at the edges of growing skull bones, and that Sp7 plays a critical role in limiting the level of signaling and the rate of bone growth. We propose a new model for how the recruitment of precursor cells and osteoblast differentiation at the sutures are coordinated to lead to proper patterning at the tissue level.

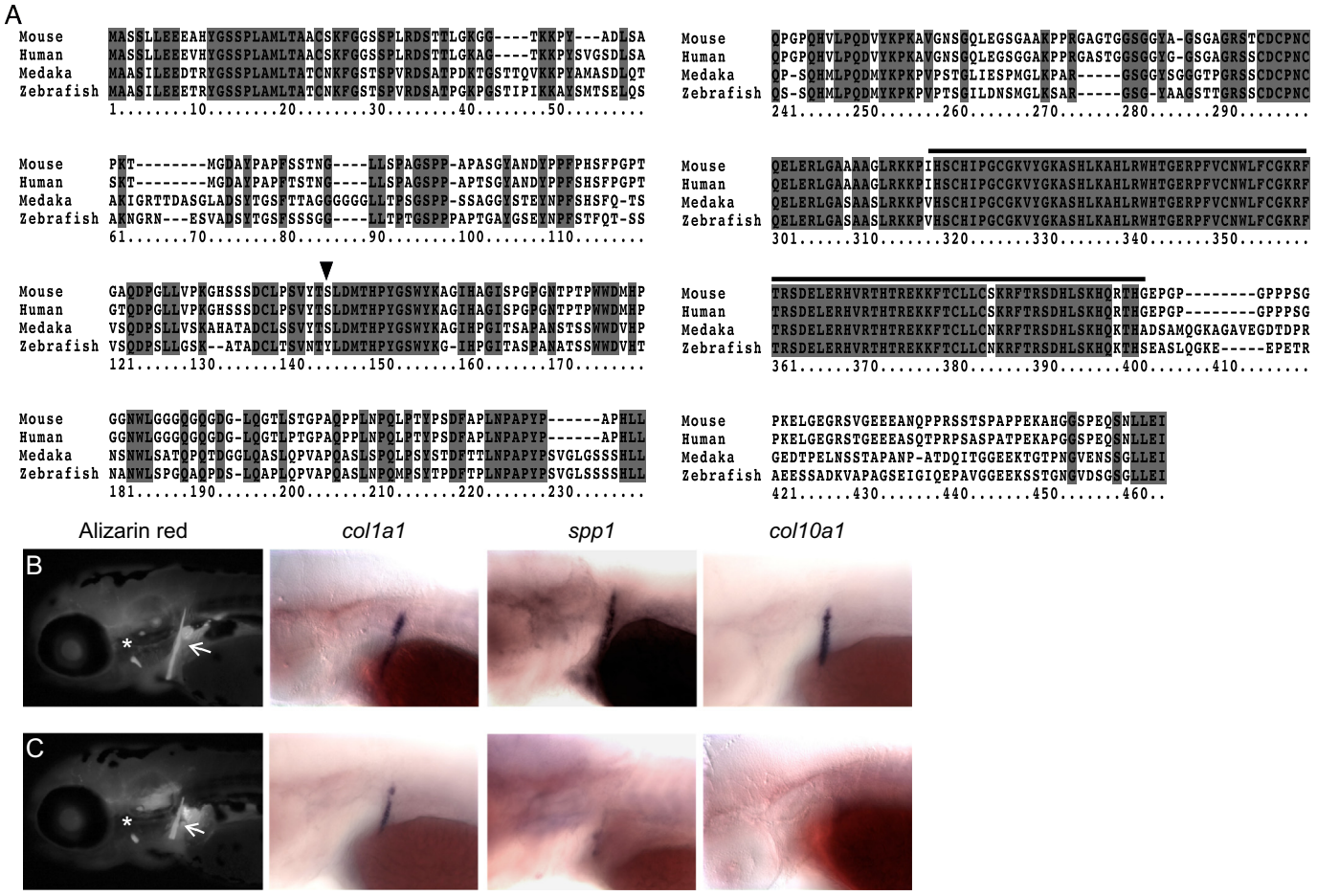

Fig. 1. Zebrafish *sp7* mutants have delayed early bone development. (A) Sp7 protein sequences of human, mouse, medaka and zebrafish were aligned using ClustalW. Identical residues are shaded dark gray. Cysteine and histidine residues corresponding to the zinc finger domains from positions 318 to 402 (black line) are highly conserved in a domain showing only three amino acid variations between mammals and fish. The mutation p.Leu145* (black triangle) introduces a stop codon, deleting over half of the Sp7 coding sequence, including the three zinc finger domains. (B and C). Calcified bones were detected at 4 dpf by vital Alizarin red staining. While WT (B) and mutant (C) larvae were indistinguishable by morphology, the cleithrum (arrows) and opercle (asterisks) are slightly smaller in *sp7* mutants. In situ hybridization was performed for markers of osteoblast differentiation in embryos at 4 dpf. Expression of all markers in the cleithrum was reduced in mutants, especially *spp1* and *col10a1*.

2. Material and methods

2.1. Zebrafish husbandry and lines

Fish were raised and maintained under standard conditions, and all studies were approved by the Institutional Animal Care and Use Committee of the University of Pennsylvania. Fish with a mutation in *sp7* were generated via target–selected ENU mutagenesis at the Hubrecht Institute (Wienholds et al., 2003), for distribution to the community. Mutation carriers were genotyped by PCR (F–cgtcaattactctttaaatctcttctc; R–aaccgcaacactaaaatcaca) followed by *Mse*I digestion. We generated transgenic fish expressing mCherry under control of *sp7* regulatory sequences (*sp7:mcherry*) using the *osterix-mcherry-BSIISK-ISce-I* plasmid (Renn and Winkler, 2009), kindly provided by Christoph Winkler. Plasmid and *Sce*I enzyme were injected into zebrafish embryos at the one cell stage to generate founders, essentially as previously described (Soroldoni et al., 2009; Thermes et al., 2002). The transgenic line expressing GFP in early osteoblasts (*Runx2:egfp*) is based on an enhancer from the human *RUNX2* gene and has been previously described (Knopf et al., 2011).

2.2. Alizarin red staining

Fish were fixed with 4% Formaldehyde overnight and Alizarin red stain performed as described (Walker and Kimmel, 2007). Alizarin red was also used to label calcified bone in live larvae as previously described (Kimmel et al., 2010).

2.3. In situ hybridization

Whole-mount in situ hybridization was carried out as described (Thisse and Thisse, 2008). For frozen sections, fish were fixed overnight in 4% paraformaldehyde and after rinsing in PBS, dissected heads were embedded in 1% agar and incubated overnight in 30% sucrose. Samples were mounted in OCT and cryosectioned, and 25 μm sections placed on TESPA-treated slides and dried at room temperature for 2 h. In situ hybridization was performed with small modifications from the whole-mount protocol. Probe templates for *spp1*, *alkaline phosphatase/alpl*, and *msx* genes were synthesized by PCR with the T7 promoter (taatacgactcactatagggag) added to reverse primers; probes were transcribed in vitro. The following primers were used: *spp1* (F–gccaatgtgttccaggttg, R gtcgctgtggtctcctcac); *alpl* (F ttgggagggaaagacaaaac, R

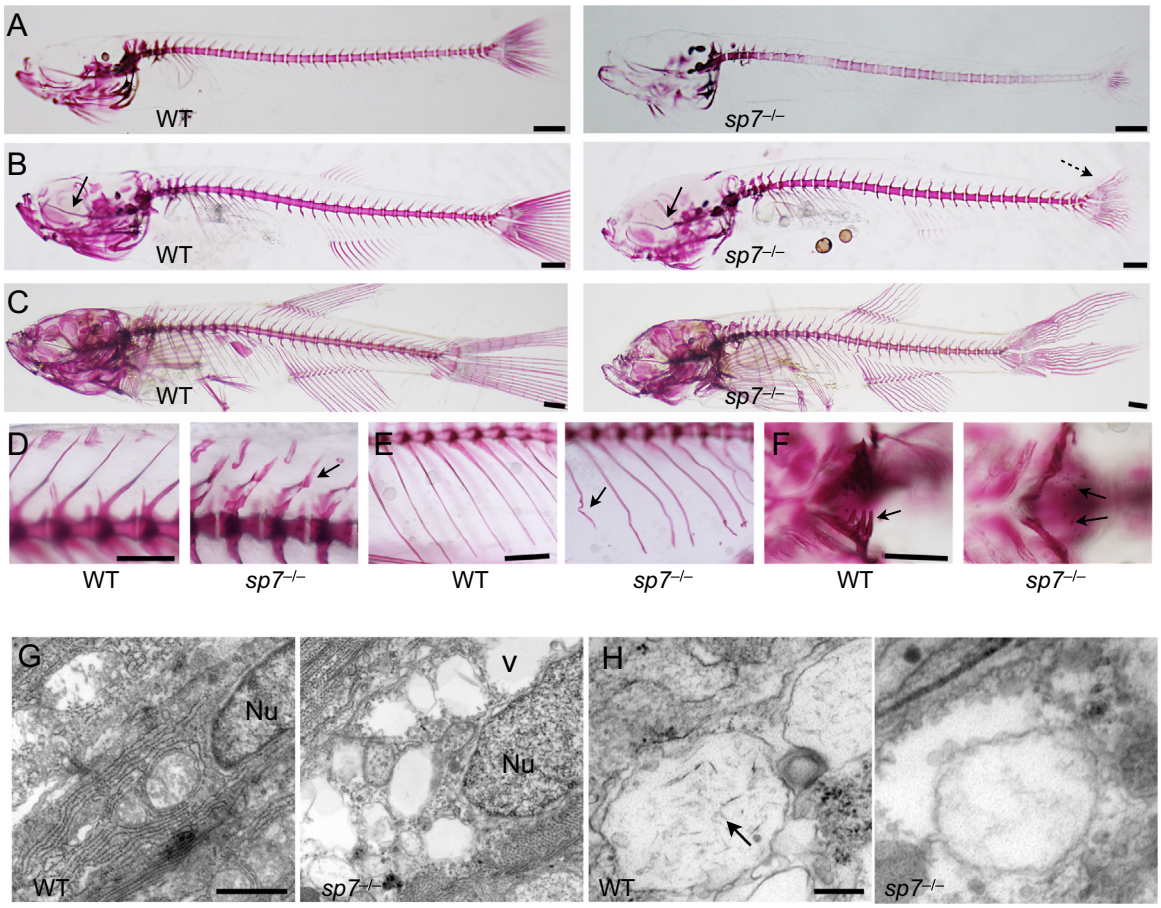

Fig. 2. *sp7* mutants show progressive skeletal malformations and deficient mineralization. (A–F) Alizarin red stain was performed on *sp7* mutants and WT siblings from 2 wpf to 8 wpf. At 2 wpf (A), the skeleton of mutants shows an overall delay in mineralization. The vertebral column is unevenly mineralized and the vertebrae weakly stained. At 4 wpf (B), mineralization in the vertebral column is similar in WT and mutant. However, the skulls of mutants start to manifest a domed shape, the parasphenoid is bent (arrow), and the caudal fin lepdotrichia are wavy (dashed arrow). At 6 wpf (C), midface hypoplasia, protruding mandible and domed skull are evident in mutants. (D) Higher magnification shows the differences in size and shape of vertebrae between WT and mutant fish at 6 wpf. Arrow indicates bending of the dorsal spinous process of a single vertebra. (E) Also at 6 wpf, ribs of mutants frequently show evidence of fractures (arrow). (F) At 4 wpf, the pharyngeal teeth in the fifth ceratobranchial are fully mineralized in WT; while present in the mutants, only the tips are mineralized (arrows). (G and H) Transmission electron microscopy was performed on parietal bones at 6 wpf. (G) The nucleus (Nu) of a normal mature osteoblast is elongated and filled with dense material. In *sp7* mutants the nuclei are rounder and filled with a less dense material. The extracellular matrix of mutant bone contains empty vacuoles (v), not observed in WT. (H) Needle-shaped hydroxyapatite crystals are present inside extracellular matrix vesicles in WT bone (arrow), but not observed in *sp7* mutants. Scale bars for A–F are 5 mm, and for G and H are 500 μm and 100 μm, respectively.

gggattgagggaaaggagat); *msxe* (F aaatttcggcagaaacagtacct, R tagttacagttcatcatctgggtca); *msxd* (F cgaaagttcagacagaaacagtacc; R aaaatgtggtggacattaaactcat); *msxb* (F tctgattggctgaaagttctattgt; R ctagagttcataacccatgatgtgc). We used previously described probes for the *twist* genes (Yeo et al., 2009) and *col10a1a* (Clement et al., 2008).

2.4. Electron microscopy

Dissected skulls at 6 wpf were fixed in 2.5% gluteraldehyde/2% paraformaldehyde. Longitudinal sections of 0.5 μm were processed at the Penn Microscopy Core Facility as follows: staining in uranyl acetate and lead citrate, one hour post-fixation in 2.0% osmium tetroxide, brief wash in dH_2O, and *en bloc* staining with 2% uranyl acetate. After ethanol dehydration, the tissue was embedded in EMbed-812 (Electron Microscopy Sciences). Ultra thin sections (70 nm) were stained with uranyl acetate and lead citrate and examined with a JEOL 1010 electron microscope fitted with a Hamamatsu digital camera and AMT Advantage image capture software.

2.5. Morphometric analysis

Fish were euthanized at 6 wpf and fixed in 4% PFA. Specimens were cleared and stained for Alizarin red, stored in 80% glycerol, and photographed in the lateral view. Geometric morphometric methods were used to assess patterns of variation in the shape of the skull of homozygous ($n=36$), heterozygous ($n=41$), and WT ($n=25$) fish using landmarks in accordance with Cubbage and Mabee (Mabee, 1996). The program tpsDig2 (Rohlf, 2006a) was

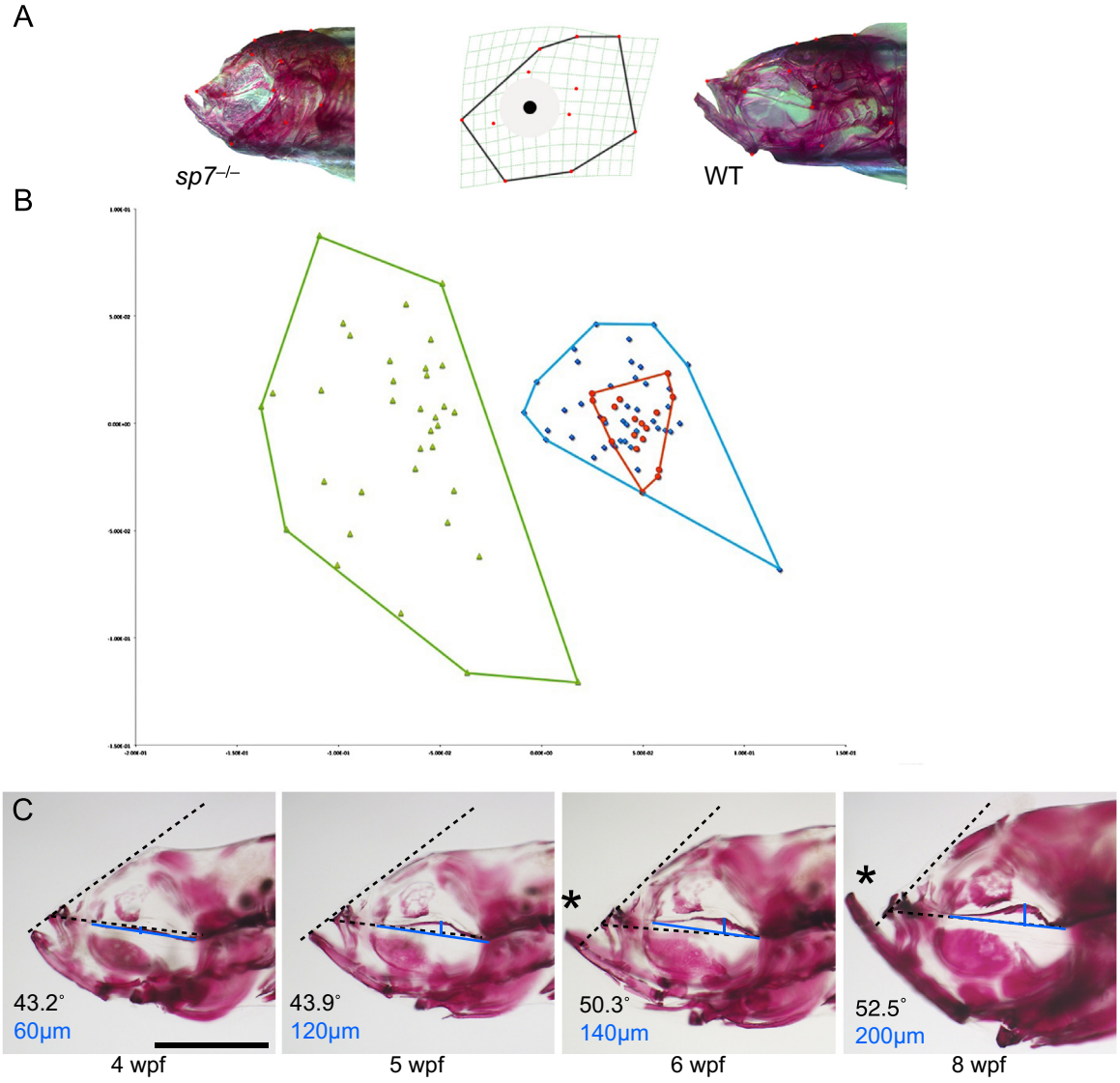

Fig. 3. Midface hypoplasia correlates with deformation of the parasphenoid. (A) 12 landmarks from the lateral view of the craniofacial skeleton of 6 wpf fish were used for morphometric analyses; representative *sp7* mutant and WT fish are shown. (B) Principal component analysis separated *sp7* homozygotes into a unique group (green). Heterozygotes group (blue) overlap with WT fish (red), although they are more variable (C) Alizarin red stained mutants representing progressive stages of craniofacial. development are shown in lateral view. Increasingly severe deformation of the parasphenoid is accompanied by midface hypoplasia. We quantified midface hypoplasia as the angle between the parasphenoid (dashed line drawn from the base of the parasphenoid to the anterior of the maxilla) and frontal bones (dashed line from the maxilla to frontal bones). In WT the angle remains nearly constant during development (data not shown), while in *sp7* mutants the angle increases (indicated at the bottom left of each picture). Asterisks indicate protrusion of the mandible as a consequence of midface hypoplasia. To quantify the deformation of the parasphenoid, we drew a line from the caudal end of the parasphenoid to its anterior (blue line) and measured the greatest distance to the bone from this line (perpendicular blue line). Note that the distance increases with the severity of hypoplasia observed (indicated at the bottom left in blue). Scale bar is 1 mm.

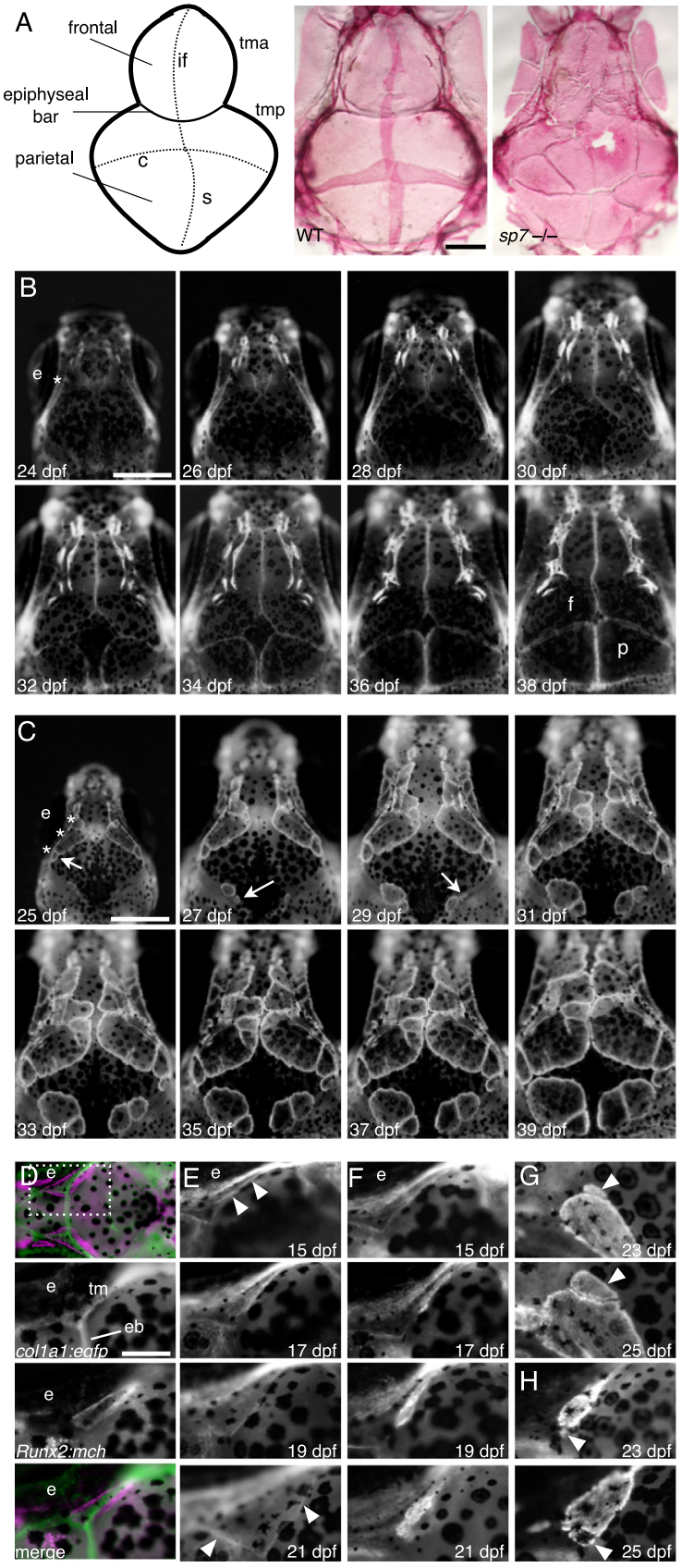
A
frontal
tma
if
epiphyseal bar
tmp
parietal
c
s
WT
sp7−/−
B
e
24 dpf
26 dpf
28 dpf
30 dpf
32 dpf
34 dpf
36 dpf
f
p
38 dpf
C
e
25 dpf
27 dpf
29 dpf
31 dpf
33 dpf
35 dpf
37 dpf
39 dpf
D
e
tm
eb
col1a1:egfp
Runx2:mch
merge
E
15 dpf
17 dpf
19 dpf
21 dpf
F
15 dpf
17 dpf
19 dpf
21 dpf
G
23 dpf
25 dpf
H
23 dpf
25 dpf

used to establish the positions of homologous anatomical landmarks on specimen images. All subsequent analyses were performed in tpsRelw (Rohlf, 2006b). A generalized procrustes analysis (Gower, 1975; Rohlf and Slice, 1990) was used to superimpose landmark configurations such that the distances between corresponding landmarks were minimized by scaling, translating, and rotating specimens with respect to a mean consensus configuration. Next, we performed a thin-plate spline analysis to obtain partial warps, which are geometrically orthogonal descriptors of shape based on scale (Rohlf and Marcus, 1993). Finally, a principal component analysis was performed on partial warp scores to identify major axes of shape variation (referred to as relative warp axes). Parsons et al. described these analyses as applied to adult zebrafish (Parsons et al., 2011).

2.6. Microarray

Fish were euthanized at 6 wpf, their skulls dissected in cold PBS, and RNA prepared in Trizol (Invitrogen). Microarray services were provided by the Penn Molecular Profiling Facility, using the Agilent Zebrafish (V3) 4×44 K microarray. Data was assembled using Partek, analyzed with Ingenuity. For generation of heat maps, an accession number list was exported from Ingenuity for genes satisfying $p \leq 0.1$ and 1.5x filters. Log2 intensities for these accession numbers were adjusted by subtracting the median (across 6 wpf samples) and then clustered using Euclidean distance with average linkage. Color indicates the difference between each gene's intensity and the median across the replicates. Differentially expressed genes involved in morphology of the skull, craniofacial abnormality, mineralization of bone and mesenchymal cell proliferation were selected using Tree view into bio Functions displayed by Ingenuity. Ingenuity Path Designer was used to create an overlapping network of molecules involved in the selected biological functions.

2.7. Immunohistochemistry

Fish were fixed overnight in 4% paraformaldehyde and cryosections performed as described above. Slides were washed twice in PBSt and blocked in 10% BSA for 1 h. Immunohistochemistry was preformed as described previously (Seiler et al., 2012). The primary antibodies anti–GFP rabbit polyclonal (Invitrogen #939306), anti-GFP mouse IgG2a (Invitrogen #1037264), anti-mCherry mouse monoclonal (Clontech #632543), anti-trimethyl-Histone H3 rabbit polyclonal (Millipore #07-449), and anti-PCNA rabbit polyclonal (Santa Cruz Biotechnology #7907) were used at a 1:500 dilution, and anti-phosphoSmad (Cell Signaling 9511L) was used at a 1:200 dilution. Secondary antibodies were used at a 1:1000 dilution: anti-rabbit Alexa fluor 594 (Invitrogen #10086648); anti-mouse Alexa Fluor 488 (Cell Signaling #4408); and anti-mouse Alexa Fluor 594 (Cell Signaling, #8890S). Sections were counterstained with DAPI (1:5000 in methanol) to reveal nuclei.

2.8. Light microscopy

For sequential live imaging, fish were anesthetized with Tricane (Sigma A-5040, 0.6 mg/mL) and mounted in a Petri dish with a well carved out of 1% agarose. Sequential pictures were taken, in the same orientation and under the same conditions, on an Olympus SZX16 microscope with DP72 camera.

3. Results

3.1. Zebrafish sp7 mutants make bone and have a normally patterned skeleton

Sp7 is highly conserved from human to zebrafish, including complete conservation of amino acid residues of the zinc finger DNA binding domain (Fig. 1A). As part of a consortium to generate target–selected zebrafish mutants (Wienholds et al., 2003), a mutation was isolated in *sp7* that introduces a stop codon at position 145, truncating the protein before the three zinc finger domains (Fig. 1A). Expression of *sp7* is an early marker of osteoblast differentiation throughout the zebrafish skeleton (DeLaurier et al., 2010; Li et al., 2009), beginning in the larval period. In the *sp7* mutants at 3 days post fertilization (dpf), the earliest forming bones, while reduced in size, were positioned normally and underwent calcification, although expression of later markers of osteogenesis (*col1a1*, *col10*, *bone sialoprotein* and *osteocalcin*) was decreased (Fig. 1B and C).

We analyzed the skeletons of *sp7* mutants and WT siblings by Alizarin red staining at standard lengths of 0.6–2.0 cm (Parichy et al., 2009), during the period from 2 to 8 wpf (Fig. 2A–F). While all skeletal elements in the mutants were initially patterned correctly, overall calcification was delayed. The axial skeleton in mutants initially was similar to that of the WT in shape (Fig. 2A). However, at later stages the dorsal spinous processes were shorter and thicker in the mutants (Fig. 2D). The lepidotrichia of the caudal fin were distorted (Fig. 2B and C), resembling a straw broom, easily recognizable in live mutants.

The craniofacial skeleton of mutants was progressively affected during this period, at later stages displaying a domed skull, midface hypoplasia, protruding mandible, and partially calcified opercle (Fig. 2C). Poor ossification was also observed in other bones in the craniofacial skeleton, i.e. pterosphenoid and orbitosphenoid, in which abnormal vacuoles were present (not shown). In addition, the pharyngeal teeth, embedded in the fifth ceratobranchial, were mineralized only at the tips (Fig. 2F).

Despite poor mineralization and the progressive changes in the craniofacial and axial skeleton during development, *sp7* mutants were viable. Adults displayed smaller overall body size, 1.8 cm compared to 2.7 cm for WT siblings. Scoliosis was present in ~75% of mutants, and fractures of the ribs were frequently observed (Fig. 2E).

Fig. 4. Multiple skull bones in *sp7* mutants arise from independent ossification sites. (A) Schematic diagram of the skull showing the flat bones (frontal and parietal), the sutures and the cartilage bars. And alizarin red stained dissected skulls from WT and *sp7* mutant fish at 6 wpf. In WT, the vault of the skull is made up of paired frontal and parietal bones that overlap by ~6 weeks to form the interfrontal, coronal, and sagittal sutures. *sp7* mutants have multiple irregular bones that fail to overlap and form normal sutures. (B and C) We followed skull formation dynamically by imaging individual *Runx2:egfp* transgenic fish every 2 days. In a WT fish (B), the frontal and parietal bones normally form as single ossifications. The position where the initiation site grows from is indicated (asterisks). In an *sp7* mutant (C), additional ossification sites arise laterally (arrows) and grow apically, giving rise to separate bones. Three initiation sites are shown with asterisks. To examine initiation of the frontal bone, we imaged transgenic fish from the earliest appearance of precursor cells. The taenia marginalis is positioned on the top of the figures (D–G). In fish doubly transgenic for a cartilage marker (*col1a1:egfp)* and *Runx2:mch*, we first observe precursor cells closely associated with the taenia marginalis anterior cartilage, just posterior to the epiphyseal bar, dashed square area (D). In WT fish (E), the cells expand in 6 days from a thin line to outline the wedge-shaped frontal bone (arrowheads). In *sp7* mutants over the same period (F), the cells instead cluster along the cartilage, and stay more closely associated during early growth. G and H illustrate from two different fish the genesis of ectopic bones (arrowheads), starting from small clusters of cells adjacent to the initial ossifications. Scale bars for A–C are 1 mm, and for D–H 0.5 mm. Abbreviations: coronal (c), epiphyseal bar (eb), eye (e), frontal (f), interfrontal (if), parietal (p), sagittal (s), taenia marginalis anterior (tma), tania marginals posterior (tmp).

3.2. Cartilage develops normally in sp7 mutants

We analyzed cartilage development in mutants by alcian blue staining of fixed samples and in live transgenic fish (Fig. S1). Initial formation of cartilage was normal, with no ectopic or missing cartilage. We also did not detect expression of *sp7* in cartilage either by in situ hybridization (data not shown) or using reporter transgenic lines based on *sp7* regulatory sequences (Fig. S1), consistent with published reports (DeLaurier et al., 2010; Li et al., 2009). In adult mutants, the joints (between the ventral hypohyals and ceratobranchials) and epiphyseal cartilages were broader (Fig. S1), but these changes were apparent concomitant with overall distortions in skull shape. Therefore, it appears that the abnormalities of cartilage in the mutants are secondary to skull shape abnormalities.

3.3. Major mineralization pathway is defective in sp7 mutants

The major bone mineralization pathway is thought to initiate inside matrix vesicles that bud off of osteoblasts, through formation of hydroxyapatite crystals (Anderson et al., 2005; Mahamid et al., 2011). The growing crystals break through the vesicles and are exposed to the extracellular matrix, where they attach to collagen fibers. Given the evidence of uneven and delayed mineralization, poor bone growth, and fragility of bone in the *sp7* mutants, we performed electron microscopy (EM) on sections of the parietal bones. In WT bone, the osteoblasts were long and narrow (Fig. 2G). The extracellular matrix showed abundant collagen fibers, and hydroxyapatite crystals were readily apparent in the matrix vesicles (Fig. 2G). In mutants, osteoblasts were rounded, consistent with a less advanced stage of differentiation, and hydroxyapatite crystals were only rarely observed in the matrix vesicles (Fig. 2H).

3.4. Midface hypoplasia correlates with deformation of parasphenoid

To better characterize the skull shape defects in the mutants, we performed a geometric morphometric shape analysis comparing the craniofacial skeletons of homozygous, heterozygous, and WT siblings (Fig. 3). In the lateral view, clear differences are noted between mutants and siblings. In the integrated skull, mutants are characterized by a dramatic truncation of the upper jaw apparatus and anterior skull, placing them in a completely separate group (Fig. 3B). Notably, while heterozygous animals are not appreciably different from WT siblings, they exhibit an increase in the variance of craniofacial shape, as depicted by the two dimensional shape space (which accounts for over 50% of the total variance) (Fig. 3B). This suggests that *sp7* haploinsufficiency affects the canalization of normal craniofacial development, resulting in a more variable skeleton.

The parasphenoid is one of the first bones to ossify in the zebrafish skull, beginning at 3 days post fertilization (dpf), and forms the base of the neurocranium housing the brain (Mabee, 1996). Later in skull growth, the parasphenoid elongates towards the nasal bone in parallel with growth of the skull. At 3–4 wpf, the skull is not yet formed and the parasphenoid in mutants is straight, as in WT fish (Fig. 3C). At 4–5 wpf, the frontal bones start to ossify as mineral deposition increases throughout the craniofacial skeleton. During this period, the parasphenoid becomes bent in mutants, corresponding with development of midface hypoplasia. The angle formed between the parasphenoid and the fontal bones is relatively constant in WT, but increases in the mutant during craniofacial development, correlating both with the severity of midface hypoplasia and the degree of parasphenoid deformation (Fig. 3C).

3.5. Sutures and skull bones are mispatterned in sp7 mutants

We examined fixed samples during skull and suture formation by whole mount Alizarin red staining. As described previously (Mabee, 1996), mineralization of the paired frontal bones is apparent ~4 wpf above the lateral extent of the epiphyseal bar cartilage, in the vicinity of the supraorbital bones. Bone formation progresses above the epiphyseal bar, toward the apex of the skull, and extends anteriorly and posteriorly. Similarly, the paired parietal bones begin forming at the posterolateral edges of the skull, and extend anteriorly and medially to cover the brain. After approximately two weeks, the membranous bones have grown to overlap each other, forming the sutures (Fig. 4A). *sp7* mutants had a striking number of extra sutures and irregular skull bones, with the area anterior to the epiphyseal bar most severely affected (Fig. 4A). Additionally, the cranial bones in the mutants did not overlap to form normal sutures, but were separated by small gaps. Although extra sutures and bones were 100% penetrant and invariably present in the mutants, we saw a broad spectrum of phenotypic variability. In some individuals, there were gaps in the skull lacking any mineralized bones, persisting to adulthood (Fig. S2). Older mutants also displayed reduced Alizarin red staining, suggesting loss of calcification with age (Fig. S2).

3.6. In vivo analysis reveals dynamics of skull bone formation

We followed skull and suture formation in *Runx2:egfp* transgenic fish, expressing GFP in early osteoblasts (Knopf et al., 2011). We imaged individual fish sequentially every 2 days during growth of the calvarial bones, from ~3.5 wpf until formation of the sutures. In WT fish over the period of imaging, the frontal and parietal bones grew steadily, with smooth edges, until they met and overlapped to form sutures (Fig. 4B). In contrast, in *sp7* mutants we observed multiple areas of GFP+cells, all of which grew concurrently to form separate bones (Fig. 4C). Additionally, the edges of the bones were more irregular in the mutants, and we could occasionally observe formation of a separate bone by a "budding" process from the edge of a larger bone (data not shown).

We similarly imaged transgenic fish from the first appearance of osteoblasts of the frontal bone, ~2 wpf. We first observed GFP+cells in a continuous line along the taenia marginalis anterior, just behind the junction with the epiphyseal bar cartilage (Fig. 4D). Over the next few days, the condensations continuously increased in area, expanding anteriorly, posteriorly, and towards the apex of the skull (Fig. 4E), with GFP expressed primarily by cells at the margins. In the *sp7* mutants, GFP+ cells were seen initially in a similar continuous line, but over a period of several days, they clustered into larger bone primordia (Fig. 4F), which although in approximately the normal location, were smaller than in WT and irregular in shape. Additional smaller clusters also formed, which gave rise to additional bones (Fig. 4G and H).

3.7. Global gene expression indicates reduced osteoblast maturation

To better understand the network of genes involved in the regulation of skull growth that are influenced directly or indirectly by *sp7*, we examined gene expression profiles through microarrays on dissected skulls at 6 wpf (Fig. 5). We found 424 genes expressed differentially (≥ 1.5 fold change, $p \leq 0.1$) between mutants and siblings (Fig. 5A), of which 104 have known functions in bone biology or morphogenesis (Fig. 5B). Of these, 73 were increased and 31 decreased in expression; significantly, genes associated with early osteoblasts were increased (*ihhb, runx2a, runx2b, twist1a, gli2, msxe, fgfr3,* and *gas1b*), while genes associated with more mature osteoblasts (*osteocalcin/bglap, col10a1a,* and *alkaline phosphatase/alpl*) showed decreased expression. We selected 26 genes

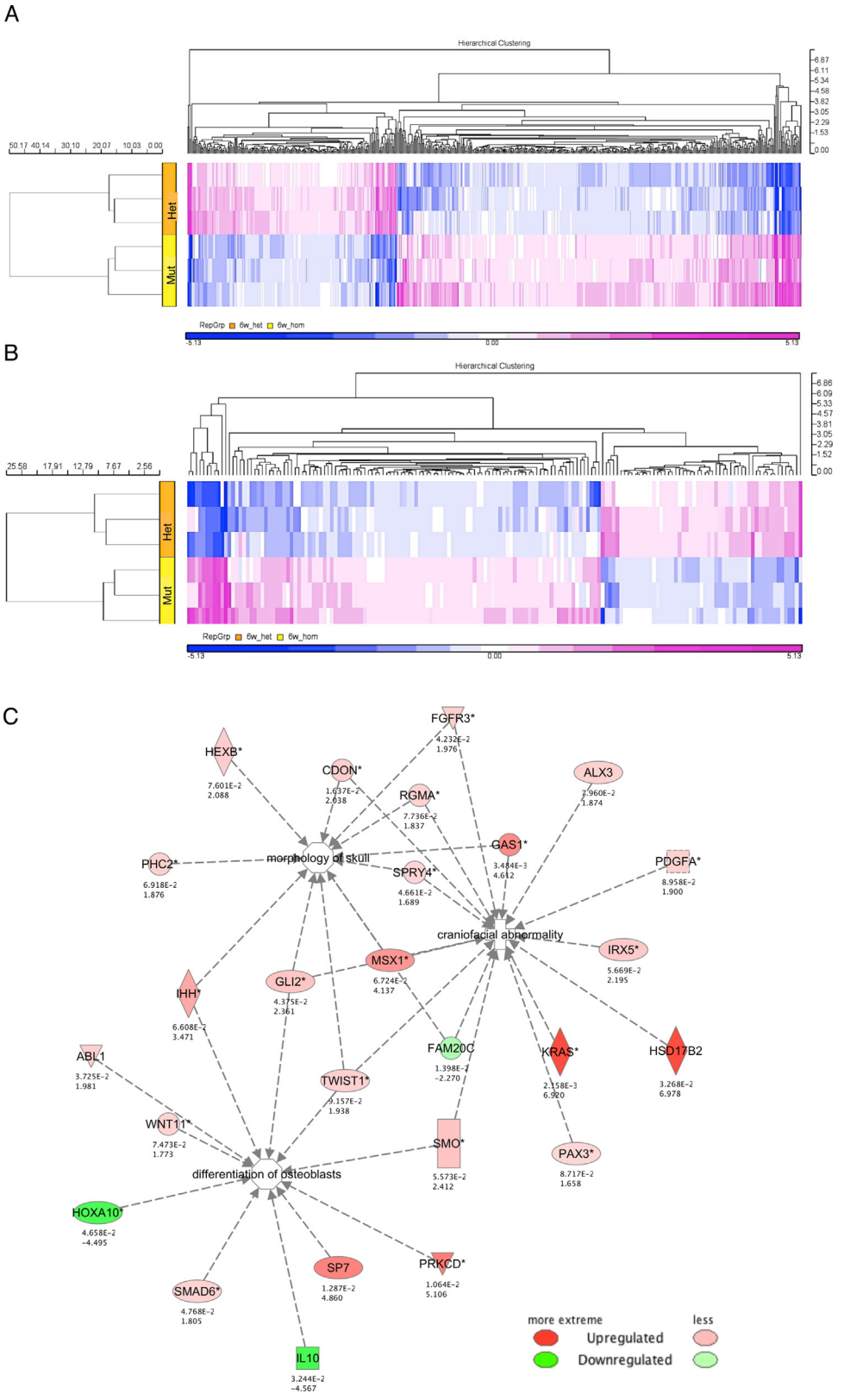

Fig. 5. *sp7* mutants have increased expression of early differentiation genes while late ostegenesis markers are decreased. (A and B) Heat maps showing differentially expressed genes clustered using Euclidean distance with average linkage. Color indicates the difference between each gene's intensity and the median across the replicates; blue indicates down-regulated genes and purple up–regulated genes. Heterozygous mutants (orange) are displayed on top and homozygous mutants (yellow) on the bottom. (A) There were a total of 424 differentially expressed genes. (B) We identified differentially expressed genes related to morphology of the skull, craniofacial abnormality, mineralization of bone and proliferation of mesenchymal cells, totaling 104 genes. (C) We created an overlapping network of the genes involved in osteoblast differentiation, skull morphology, and craniofacial abnormality. Genes in the *msx*, *twist*, and *gli* families, all up-regulated in the mutants, linked all three categories. Note that *sp7* transcript is unregulated in the mutant, what would be expected as a feedback loop in attempt to maintain the levels of the protein.

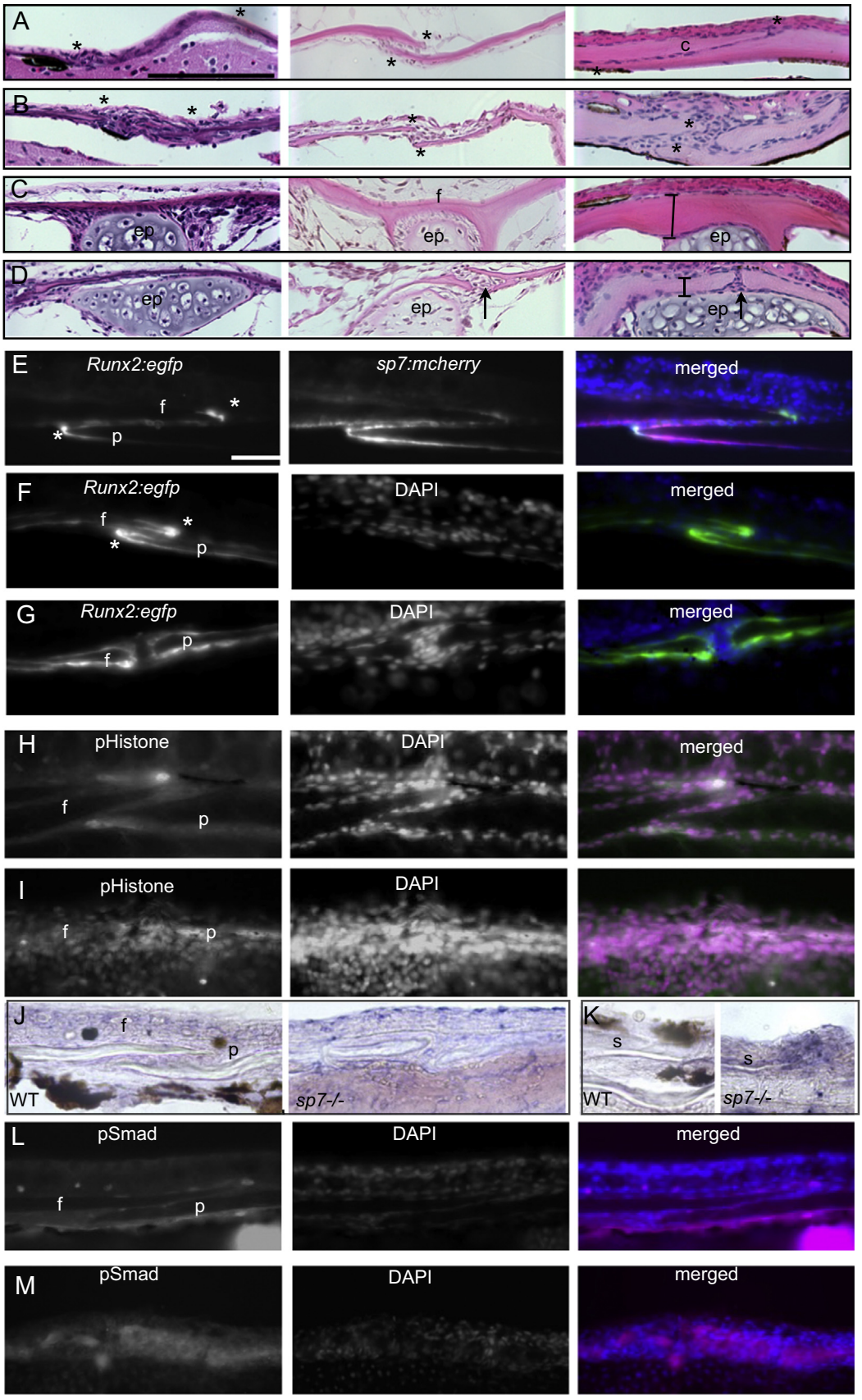
A
B
C
ep
f
D
ep
E
Runx2:egfp
f
p
sp7:mcherry
merged
F
Runx2:egfp
DAPI
merged
G
Runx2:egfp
DAPI
merged
H
pHistone
DAPI
merged
I
pHistone
DAPI
J
WT
sp7-/-
K
s
WT
sp7-/-
L
pSmad
DAPI
merged
M
pSmad
DAPI
merged

related to the categories of skull morphology, craniofacial abnormalities, and osteoblast differentiation to build a network using Ingenuity Path Designer (Fig. 5C). Among the genes displayed in the network, members of the *twist*, *gli*, and *msx* gene families connect all three categories.

3.8. Abnormal tissue architecture distinguishes suture formation in sp7 mutants

We have divided the process of suture formation into three phases, which can be observed in histological sections through the coronal sutures (Fig. 6A). During the initiation phase, the flat bones are separated by a large gap of undifferentiated cells ($>25\ \mu m$) and face each other with approximately 0° of inclination. During the approximation phase, when the bones have grown to within 25 μm, the opposing osteogenic fronts display inclinations of roughly 45°. In the final, overlapping phase, the flat bones completely overlap and a thin layer of cells separates the internal surface of the top bone from the external surface of the bottom bone.

The morphology of the sutures in *sp7* mutants was similar to WT during the initiation phase (Fig. 6B). During the approximation phase, the osteogenic fronts became thickened and rounded in the mutants, while the flat bones behind the fronts were thinner than WT. During the overlapping phase, the osteogenic fronts were even thicker and more rounded. They never overlapped, and remained separated by mesenchymal cells (Fig. 6B). In WT fish, the frontal bones overlying the epiphyseal bar cartilage are ~14 μm during the approximation phase, increasing to ~27 μm during the overlapping phase (Fig. 6C), while in mutants the frontal bones are at least 2 fold thinner, ~4 and 11 μm, at the same stages (Fig. 6D).

3.9. Sp7 is required for maturation and control of proliferation of early osteoblasts

We examined osteoblast differentiation at the coronal suture in fish carrying the *Runx2:egfp* transgene and an *sp7:mcherry* transgene. In WT fish, sutures at the approximation stage show clusters of strongly GFP+ early osteoblasts at the osteogenic fronts; as the cells differentiate, transgene expression decreases along the bones (Fig. 6E and F). For *sp7:mcherry*, the opposite is observed, with increased expression in cells farther from the osteogenic fronts (Fig. 6E). The transgenes are co-expressed in a few cells proximal to the osteogenic fronts (Fig. 6E). In *sp7* mutants, GFP+ cells are not limited to the osteogenic fronts and are abundant along the flat bones, suggesting that Sp7 is required for the normal progression of osteoblast differentiation (Fig. 6G). We also examined cell proliferation at the sutures, using antibodies against phosphohistone H3 and proliferating cell nuclear antigen (PCNA) (Fig. 6H and I and data not shown). At WT sutures, proliferating cells were seen in the early osteoblasts at the osteogenic fronts, but almost never among the mesenchymal cells within the suture (Fig. 6H). In *sp7* mutants, despite the increase in the mesenchymal cell population, we observed no apparent increase in proliferation in those cells. However, the cells associated with the bones, corresponding to the expanded population of GFP+ early osteoblasts, had a greatly increased proportion of proliferating cells (Fig. 6I).

3.10. Sp7 limits BMP signaling at the sutures

Of the common genes identified in the microarray network, *Msx* and *Twist* genes are implicated in the regulation of sutural mesenchymal cells, but are thought to have distinct roles based on human mutant phenotypes. While the *Msx* genes are thought to promote osteoblast differentiation, *Twist* genes are thought to favor maintenance of undifferentiated mesenchymal cells (Bildsoe et al., 2013; Han et al., 2007; Isenmann et al., 2009; Ishii et al., 2003). Therefore, we examined expression of all members of these gene families in zebrafish (four *twist* genes and five *msx* genes) by *in situ* hybridization on sections through the coronal suture, in WT and *sp7* mutant fish. Only for *msxd*, one of the zebrafish orthologues of *Msx2* (Postlethwait, 2006), was there a significant difference in mutants, with greatly increased expression in mesenchymal cells at the suture (Fig. 6J and K). *msxd* expression was also highly increased at the scales (Fig. S3). Since *Msx* genes are known to be regulated by BMP signaling (Maxson and Ishii, 2008), we examined phosphorylation of Smad 4/5 as a more direct measure of BMP activity. Consistent with an increase in BMP signaling, we observe a broad increase in pSmad+ nuclei surrounding the osteogenic fronts at the coronal suture in *sp7* mutants (Fig. 6L and M).

4. Discussion

The growth of the skull and formation of sutures offers a unique paradigm to explore the regulation of bone formation. The coordination between the stereotyped structure of the sutures and the orderly growth of the cranial bones is highly conserved in evolution, often disrupted in disease, yet incompletely understood at the molecular level. Because of its easy accessibility during development, the zebrafish offers unparalleled opportunities for imaging dynamic processes even in adults. We have exploited the power of live imaging to describe the initiation and growth of skull bones in zebrafish, and the skull patterning abnormalities that arise in mutants lacking Sp7, with a primary defect in osteoblast differentiation. Distinctively from mice knockout that die just after birth, our data permits characterization of the craniofacial skeleton and support a new hypothesis for the regulation of skull bone growth, where signaling from more mature bone limits the recruitment of new osteoblasts at the osteogenic fronts. We also describe one mechanism underlying the formation of ectopic, or Wormian, skull bones, a poorly understood component of many human craniofacial defects.

Sp7/Osterix was first identified as a gene increased in response to BMP signaling in cell culture, expressed specifically in the developing skeleton, and required for osteoblast differentiation in the mouse (Nakashima et al., 2002). Subsequent conditional

Fig. 6. Sutures of *sp7* mutants show abnormal architecture and gene expression. (A–D) Tissue morphology was assessed by hematoxylin-eosin staining of sagittal sections of the skull to show the coronal suture. In WT (A), suture formation is divided into three progressive phases as the osteogenic fronts (*) approach and overlap: initiation (~4 weeks), approximation (~5 weeks), and overlapping (> 6 weeks). In *sp7* mutants (B), initiation and approximation phases are similar to WT, but overlapping does not occur, and osteogenic fronts have a rounded shape. During the same period, the frontal bone above the epiphyseal bar cartilage (eb) increases in thickness (C), but in *sp7* mutants (D) the frontal bones are thinner (brackets in C and D), and extra sutures are common (arrows). (E–I) Tissue sections from transgenic fish were analyzed by immunohistochemistry for GFP, mCherry, and phosphohistone H3. In WT fish (E), expression of the *Runx2:egfp* transgene is confined to cells at the osteogenic front, while *sp7:mcherry* expression is maintained in cells along the bone; both transgenes are expressed at the osteogenic fronts (asterisks). Immature osteoblasts expressing *Runx2* (GFP+) are observed at the osteogenic fronts of WT fish (F) while in mutants these cells are not limited to the fronts (G). Proliferation was analyzed in WT (H) and *sp7* mutant (I) fish. Phosphohistone H3+cells were more frequently observed at the osteogenic fronts in mutants, and these corresponded to the GFP+ early osteoblasts (merge). (J and K) Expression of *msxd* (J) at the coronal suture and scales (K) was examined by in situ hybridization in WT and *sp7-/-;* expression was significantly increased in mesenchymal cells of mutants. (L and M) To examine the level of BMP signaling, sections were analyzed with an antibody to phosphorylated Smad 1/4/5. Numbers of pSmad+ nuclei in and around the suture were much greater in *sp7* mutants (M). Scale bars for all panels are 50 μm. Abbreviations: epiphyseal bar cartilage (eb), frontal bone (f), parietal bone (p), scale (s).

inactivation of the mouse gene at later stages in development suggests that although there is an ongoing requirement for the gene in bone homeostasis, it is not absolutely required for bone formation (Baek et al., 2010). The *sp7* gene has also been knockdown during early development in medaka (Renn and Winkler, 2014), through antisense morpholinos. It is not required for bone formation in the early embryo, but rather its loss delays osteoblast maturation. Similarly, although in our genetic mutant we do find a specific requirement for *sp7* in zebrafish skeletal development, it is not necessary for bone formation. While we cannot rule out a more absolute requirement for *Sp7* in mammalian osteogenesis, the preponderance of evidence suggests that its primary function across a number of species is to promote osteoblast differentiation. Interestingly, there is no evidence of an *Sp7* homologue in the chicken genome, further supporting the idea that it is not required for bone formation.

A human patient originally diagnosed with severe recessive osteogenesis imperfecta has been identified with a homozygous single base pair deletion in *OSTERIX/SP7*, which frameshift mutation removes the last zinc finger domain of the protein (Lapunzina et al., 2010). The human patient displayed many features that we observe in the zebrafish *sp7* mutants, including poor bone growth, a propensity for fractures, and specific craniofacial defects (midface hypoplasia, Wormian skull bones), demonstrating that the present zebrafish mutant lacking all three zinc fingers domains represents an accurate model for the human mutation.

The suture is exquisitely sensitive to perturbations in the process of osteoblast differentiation, as evidenced by human mutations leading to cranial suture defects. It is generally thought that mutations that accelerate osteoblast differentiation lead to craniosynostosis, while those that delay differentiation are associated with delayed bone growth and open fontenelles (Morriss-Kay and Wilkie, 2005). Human *MSX2* mutations fit into this framework, with gain of function mutations leading to craniosynostosis (Florisson et al., 2013; Jabs et al., 1993), while haploinsufficiency causes slow growth of the skull bones and delayed closure of the fontanels (Wilkie et al., 2000). Since Sp7 promotes osteoblast differentiation, its loss might be expected to lead to a similar phenotype. However, although the sutures fail to overlap in the mutants, they display neither craniosynostosis nor delayed closure of the fontanels. Instead, the predominant defect is a striking mispatterning of cranial bones, with the normal frontal and parietal bones almost completely replaced by a random mosaic of smaller bones.

The formation of calvarial bones can be divided broadly into three processes: the initiation of bone formation, rapid growth at the edges as the bones approximate, and a slower phase of growth once they have overlapped to form sutures. The signals responsible for initiation of calvarial bones are currently unknown. We used sequential live imaging to examine the earliest development of the frontal bones, and first observe a small number of early osteoblasts aligned adjacent to cartilage in the supraorbital region. Sp7 is not required for the first signal inducing these early osteoblasts. However, shortly following induction of the frontal and parietal bones, the *sp7* mutants show additional, nearby but separate, areas of ossification, where we observe abnormal distribution and clustering of early osteoblasts. Since *sp7* expression is confined to differentiating osteoblasts, its loss cannot directly affect the mesenchymal cells responding to an inducing signal. Instead, we hypothesize that the immature osteoblasts signal to recruit additional nearby cells (Fig. 7A). As the osteoblasts differentiate under the control of Sp7, signaling is limited. In the absence of Sp7, excess cells are recruited, leading to ectopic sites of ossification and extra bones.

The rapid growth phase of the cranial bones can be computationally modeled by assuming the existence of a single signaling source, and a field of cells competent to respond in the vicinity of the source (Garzon-Alvarado, 2014; Garzon-Alvarado et al., 2013). According to our model, in the *sp7* mutants each ossification center is a separate signaling source, which in turn signals to the surrounding

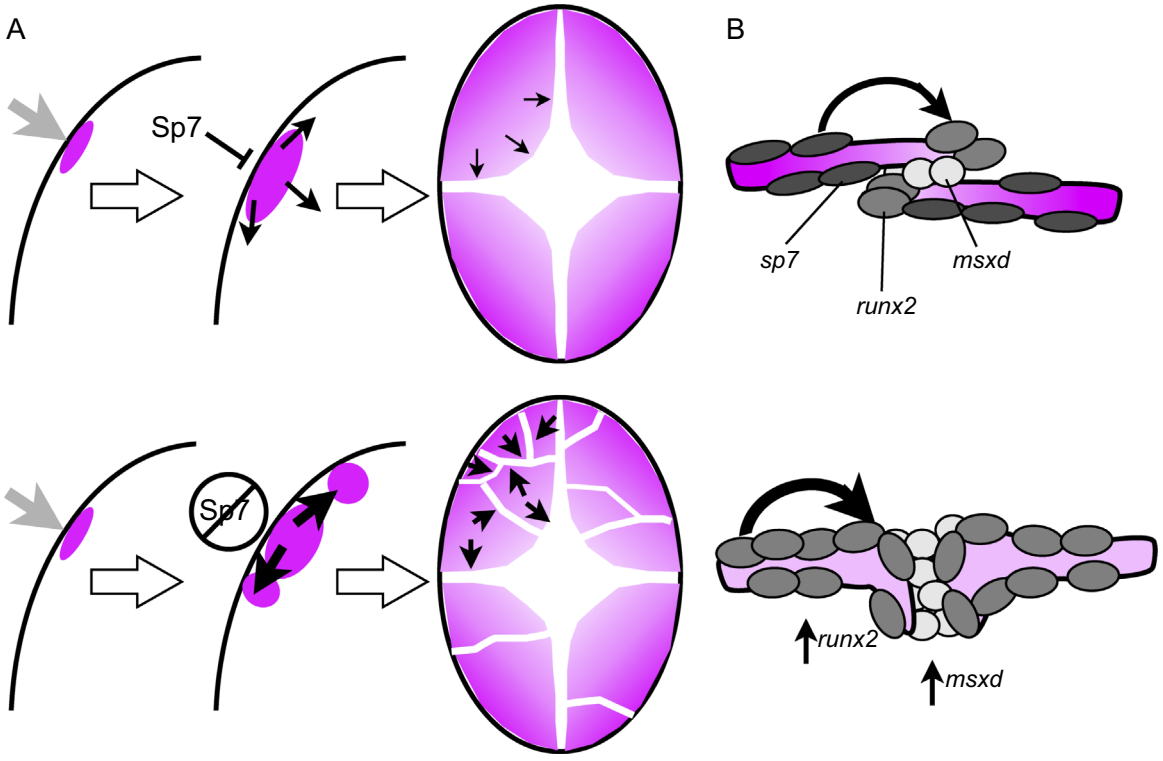

Fig. 7. Model of Sp7 requirement for regulated skull growth. (A) After induction of the frontal bone, Sp7 limits the signal from the bone itself recruiting new osteoblasts. In its absence, excess signaling leads to ectopic initiation sites. Increased signaling persists as the bones grow, leading to abnormal architecture of the osteogenic fronts. (B) At the microscopic level, loss of Sp7 prevents the orderly differentiation of osteoblasts away from the osteogenic fronts, and leads to a highly proliferative population of early osteoblasts, abnormal shape of the bone edges, and an accumulation of mid-sutural mesenchymal cells.

cells, recruiting more osteoblasts and resulting in positive feedback and worsening of the phenotype. Furthermore, the increase in *msxd* expression and pSmad+ nuclei implicates BMP signaling as the major pathway for new osteoblast recruitment.

There is a continued requirement for Sp7 during the final phase of suture formation and slower growth. As the calvarial bones grow towards each other, the architecture at the sutures becomes increasingly abnormal in mutants. Their increased thickness at the edges is accompanied by a large number of highly proliferative early osteoblasts, suggesting that the amount of bone matrix deposited at the growing edge of the skull bones is proportional to the number of proliferating early precursors. The bones ultimately fail to overlap and form normal sutures. The abnormal thickness at the edges may present a mechanical barrier to the overlap, although abnormal signaling at the sutures could also contribute. Future experiments may distinguish between these possibilities.

We propose that Sp7, and bone-derived BMP signaling regulated by it, are part of a critical feedback loop whereby mature bone controls the rate of new bone formation at the nearby osteogenic fronts. When feedback is interrupted in the *sp7* mutants, the resulting misregulation leads to increased recruitment of early osteoblasts, formation of ectopic areas of ossification, and increased deposition of matrix at the edges of the bones (Fig. 7B). This is accompanied by increased expression of *msxd*, although *Msx* gene overexpression in other settings leads to craniosynostosis. In mouse, conditional mutations of *Msx1* and *Msx2* in neural crest lead to ectopic skull bone formation, and the authors ascribed a role to the *Msx* genes in suppressing ectopic bone formation (Roybal et al., 2010). They also observed an overall increase in BMP signaling, consistent with our model of a feedback loop. Although our data does not support a major role for the *Msx* genes in suppressing formation of ectopic skull bones, future studies may identify other downstream genes that contribute to ectopic bone formation in the setting of increased BMP signaling. Our analysis of suture formation in the absence of Sp7 demonstrates that changes in osteoblast differentiation are not inextricably linked to either craniosynostosis or delayed suture closure, and importantly supports a new hypothesis for how osteoblast differentiation, recruitment of precursor cells, growth of bones, and establishment of sutures are coordinated during skull development.

Acknowledgments

We acknowledge National Institute of Dental & Craniofacial Research (NIDCR) for funding (1U01DE024434 and R21DE021509). We thank Dr. Maria Rita dos Santos Passos-Bueno and Dr. Richard Behringer for proofreading the manuscript and support.

Appendix A. Supplementary material

Supplementary data associated with this article can be found in the online version at http://dx.doi.org/10.1016/j.ydbio.2016.03.011.

References

Anderson, H.C., Garimella, R., Tague, S.E., 2005. The role of matrix vesicles in growth plate development and biomineralization. Front. Biosci. 10, 822–837.
Baek, W.Y., de Crombrugghe, B., Kim, J.E., 2010. Postnatally induced inactivation of Osterix in osteoblasts results in the reduction of bone formation and maintenance. Bone 46, 920–928.
Bellary, S.S., Steinberg, A., Mirzayan, N., Shirak, M., Tubbs, R.S., Cohen-Gadol, A.A., Loukas, M., 2013. Wormian bones: a review. Clin. Anat. 26, 922–927.
Bildsoe, H., Loebel, D.A., Jones, V.J., Hor, A.C., Braithwaite, A.W., Chen, Y.T., Behringer, R.R., Tam, P.P., 2013. The mesenchymal architecture of the cranial mesoderm of mouse embryos is disrupted by the loss of Twist1 function. Dev. Biol. 374, 295–307.
Clement, A., Wiweger, M., von der Hardt, S., Rusch, M.A., Selleck, S.B., Chien, C.B., Roehl, H.H., 2008. Regulation of zebrafish skeletogenesis by ext2/dackel and papst1/pinscher. PLoS Genet. 4, e1000136.
Cremin, B., Goodman, H., Spranger, J., Beighton, P., 1982. Wormian bones in osteogenesis imperfecta and other disorders. Skelet. Radiol. 8, 35–38.
DeLaurier, A., Eames, B.F., Blanco-Sanchez, B., Peng, G., He, X., Swartz, M.E., Ullmann, B., Westerfield, M., Kimmel, C.B., 2010. Zebrafish sp7:EGFP: a transgenic for studying otic vesicle formation, skeletogenesis, and bone regeneration. Genesis 48, 505–511.
Florisson, J.M., Verkerk, A.J., Huigh, D., Hoogeboom, A.J., Swagemakers, S., Kremer, A., Heijsman, D., Lequin, M.H., Mathijssen, I.M., van der Spek, P.J., 2013. Boston type craniosynostosis: report of a second mutation in MSX2. Am. J Med. Genet. A 161A, 2626–2633.
Garzon-Alvarado, D.A., 2014. A biochemical strategy for simulation of endochondral and intramembranous ossification. Comput. Methods Biomech. Biomed. Eng. 17, 1237–1247.
Garzon-Alvarado, D.A., Gonzalez, A., Gutierrez, M.L., 2013. Growth of the flat bones of the membranous neurocranium: a computational model. Comput. Methods Prog. Biomed. 112, 655–664.
Gower, J.C., 1975. Generalized procrustes analysis. Psychometrika 40, 33–51.
Han, J., Ishii, M., Bringas Jr., P., Maas, R.L., Maxson Jr., R.E., Chai, Y., 2007. Concerted action of Msx1 and Msx2 in regulating cranial neural crest cell differentiation during frontal bone development. Mech. Dev. 124, 729–745.
Isenmann, S., Arthur, A., Zannettino, A.C., Turner, J.L., Shi, S., Glackin, C.A., Gronthos, S., 2009. TWIST family of basic helix-loop-helix transcription factors mediate human mesenchymal stem cell growth and commitment. Stem Cells 27, 2457–2468.
Ishii, M., Merrill, A.E., Chan, Y.S., Gitelman, I., Rice, D.P., Sucov, H.M., Maxson Jr., R.E., 2003. Msx2 and Twist cooperatively control the development of the neural crest-derived skeletogenic mesenchyme of the murine skull vault. Development 130, 6131–6142.
Jabs, E.W., Muller, U., Li, X., Ma, L., Luo, W., Haworth, I.S., Klisak, I., Sparkes, R., Warman, M.L., Mulliken, J.B., et al., 1993. A mutation in the homeodomain of the human MSX2 gene in a family affected with autosomal dominant craniosynostosis. Cell 75, 443–450.
Kimmel, C.B., DeLaurier, A., Ullmann, B., Dowd, J., McFadden, M., 2010. Modes of developmental outgrowth and shaping of a craniofacial bone in zebrafish. PLoS One 5, e9475.
Knopf, F., Hammond, C., Chekuru, A., Kurth, T., Hans, S., Weber, C.W., Mahatma, G., Fisher, S., Brand, M., Schulte-Merker, S., Weidinger, G., 2011. Bone regenerates via dedifferentiation of osteoblasts in the zebrafish fin. Dev. Cell. 20, 713–724.
Lapunzina, P., Aglan, M., Temtamy, S., Caparros-Martin, J.A., Valencia, M., Leton, R., Martinez-Glez, V., Elhossini, R., Amr, K., Vilaboa, N., Ruiz-Perez, V.L., 2010. Identification of a frameshift mutation in Osterix in a patient with recessive osteogenesis imperfecta. Am. J Hum. Genet. 87, 110–114.
Laue, K., Pogoda, H.M., Daniel, P.B., van Haeringen, A., Alanay, Y., von Ameln, S., Rachwalski, M., Morgan, T., Gray, M.J., Breuning, M.H., Sawyer, G.M., Sutherland-Smith, A.J., Nikkels, P.G., Kubisch, C., Bloch, W., Wollnik, B., Hammerschmidt, M., Robertson, S.P., 2011. Craniosynostosis and multiple skeletal anomalies in humans and zebrafish result from a defect in the localized degradation of retinoic acid. Am. J Hum. Genet. 89, 595–606.
Lee, B., Thirunavukkarasu, K., Zhou, L., Pastore, L., Baldini, A., Hecht, J., Geoffroy, V., Ducy, P., Karsenty, G., 1997. Missense mutations abolishing DNA binding of the osteoblast-specific transcription factor OSF2/CBFA1 in cleidocranial dysplasia. Nat. Genet. 16, 307–310.
Li, N., Felber, K., Elks, P., Croucher, P., Roehl, H.H., 2009. Tracking gene expression during zebrafish osteoblast differentiation. Dev. Dyn. 238, 459–466.
Mabee, C.C.Ca.P.M., 1996. Development of the cranium and paired fins in the zebrafish Danio rerio (Osariophysi, Cyprinidae). J. Morphol. 229, 121–160.
Mahamid, J., Sharir, A., Gur, D., Zelzer, E., Addadi, L., Weiner, S., 2011. Bone mineralization proceeds through intracellular calcium phosphate loaded vesicles: a cryo-electron microscopy study. J Struct. Biol. 174, 527–535.
Marti, B., Sirinelli, D., Maurin, L., Carpentier, E., 2013. Wormian bones in a general paediatric population. Diagn. Interv. Imaging 94, 428–432.
Maxson, R., Ishii, M., 2008. The Bmp pathway in skull vault development. Front. Oral. Biol. 12, 197–208.
Miura, S., Hanaoka, K., Togashi, S., 2008. Skeletogenesis in Xenopus tropicalis: characteristic bone development in an anuran amphibian. Bone 43, 901–909.
Morriss-Kay, G.M., Wilkie, A.O., 2005. Growth of the normal skull vault and its alteration in craniosynostosis: insights from human genetics and experimental studies. J. Anat. 207, 637–653.
Nakashima, K., Zhou, X., Kunkel, G., Zhang, Z., Deng, J.M., Behringer, R.R., de Crombrugghe, B., 2002. The novel zinc finger-containing transcription factor osterix is required for osteoblast differentiation and bone formation. Cell 108, 17–29.
O'Loughlin, V.D., 2004. Effects of different kinds of cranial deformation on the incidence of wormian bones. Am. J Phys. Anthropol. 123, 146–155.
Otto, F., Kanegane, H., Mundlos, S., 2002. Mutations in the RUNX2 gene in patients with cleidocranial dysplasia. Hum. Mutat. 19, 209–216.
Parichy, D.M., Elizondo, M.R., Mills, M.G., Gordon, T.N., Engeszer, R.E., 2009. Normal table of postembryonic zebrafish development: staging by externally visible anatomy of the living fish. Dev. Dyn. 238, 2975–3015.
Parsons, T.E., Schmidt, E.J., Boughner, J.C., Jamniczky, H.A., Marcucio, R.S., Hallgrimsson, B., 2011. Epigenetic integration of the developing brain and face. Dev. Dyn. 240, 2233–2244.
Postlethwait, J.H., 2006. The zebrafish genome: a review and msx gene case study. Genome Dyn. 2, 183–197.
Quarto, N., Longaker, M.T., 2005. The zebrafish (*Danio rerio*): a model system for cranial suture patterning. Cells Tissues Organs 181, 109–118.

Renn, J., Winkler, C., 2009. Osterix-mCherry transgenic medaka for in vivo imaging of bone formation. Dev. Dyn. 238, 241–248.
Renn, J., Winkler, C., 2014. Osterix/Sp7 regulates biomineralization of otoliths and bone in medaka (Oryzias latipes). Matrix Biol. 34, 193–204.
Rivadeneira, F., Styrkarsdottir, U., Estrada, K., Halldorsson, B.V., Hsu, Y.H., Richards, J. B., Zillikens, M.C., Kavvoura, F.K., Amin, N., Aulchenko, Y.S., Cupples, L.A., Deloukas, P., Demissie, S., Grundberg, E., Hofman, A., Kong, A., Karasik, D., van Meurs, J.B., Oostra, B., Pastinen, T., Pols, H.A., Sigurdsson, G., Soranzo, N., Thorleifsson, G., Thorsteinsdottir, U., Williams, F.M., Wilson, S.G., Zhou, Y., Ralston, S.H., van Duijn, C.M., Spector, T., Kiel, D.P., Stefansson, K., Ioannidis, J.P., Uitterlinden, A.G., Genetic Factors for Osteoporosis, C., 2009. Twenty bone-mineral-density loci identified by large-scale meta-analysis of genome-wide association studies. Nat. Genet. 41, 1199–1206.
Rohlf, F.J., 2006a. tpsDIG2 software for morphometric analysis ⟨http://life.bio.sunysb.edu/morph/⟩.
Rohlf, F.J., 2006b. tpsRelw software for morphometric analysis ⟨http://life.bio.sunysb.edu/morph/⟩.
Rohlf, F.J., Marcus, L.F., 1993. A revolution in morphometrics. Trends Ecol. Evol. 8, 129–132.
Rohlf, F.J., Slice, D.E., 1990. Extensions of the procrustes method for the optimal superimposition of landmarks. Syst. Zool. 39, 40–59.
Roybal, P.G., Wu, N.L., Sun, J., Ting, M.C., Schafer, C.A., Maxson, R.E., 2010. Inactivation of Msx1 and Msx2 in neural crest reveals an unexpected role in suppressing heterotopic bone formation in the head. Dev. Biol. 343, 28–39.
Sanchez-Lara, P.A., Graham Jr., J.M., Hing, A.V., Lee, J., Cunningham, M., 2007. The morphogenesis of wormian bones: a study of craniosynostosis and purposeful cranial deformation. Am. J Med. Genet. A 143A, 3243–3251.
Seiler, C., Davuluri, G., Abrams, J., Byfield, F.J., Janmey, P.A., Pack, M., 2012. Smooth muscle tension induces invasive remodeling of the zebrafish intestine. PLoS Biol. 10, e1001386.
Soroldoni, D., Hogan, B.M., Oates, A.C., 2009. Simple and efficient transgenesis with meganuclease constructs in zebrafish. Methods Mol. Biol. 546, 117–130.
Styrkarsdottir, U., Halldorsson, B.V., Gretarsdottir, S., Gudbjartsson, D.F., Walters, G. B., Ingvarsson, T., Jonsdottir, T., Saemundsdottir, J., Snorradottir, S., Center, J.R., Nguyen, T.V., Alexandersen, P., Gulcher, J.R., Eisman, J.A., Christiansen, C., Sigurdsson, G., Kong, A., Thorsteinsdottir, U., Stefansson, K., 2009. New sequence variants associated with bone mineral density. Nat. Genet. 41, 15–17.
Thermes, V., Grabher, C., Ristoratore, F., Bourrat, F., Choulika, A., Wittbrodt, J., Joly, J. S., 2002. I-SceI meganuclease mediates highly efficient transgenesis in fish. Mech. Dev. 118, 91–98.
Thisse, C., Thisse, B., 2008. High-resolution in situ hybridization to whole-mount zebrafish embryos. Nat. Protoc. 3, 59–69.
Timpson, N.J., Tobias, J.H., Richards, J.B., Soranzo, N., Duncan, E.L., Sims, A.M., Whittaker, P., Kumanduri, V., Zhai, G., Glaser, B., Eisman, J., Jones, G., Nicholson, G., Prince, R., Seeman, E., Spector, T.D., Brown, M.A., Peltonen, L., Smith, G.D., Deloukas, P., Evans, D.M., 2009. Common variants in the region around Osterix are associated with bone mineral density and growth in childhood. Hum. Mol. Genet. 18, 1510–1517.
Walker, M.B., Kimmel, C.B., 2007. A two-color acid-free cartilage and bone stain for zebrafish larvae. Biotech. Histochem. 82, 23–28.
Wienholds, E., van Eeden, F., Kosters, M., Mudde, J., Plasterk, R.H., Cuppen, E., 2003. Efficient target-selected mutagenesis in zebrafish. Genome Res. 13, 2700–2707.
Wilkie, A.O., Tang, Z., Elanko, N., Walsh, S., Twigg, S.R., Hurst, J.A., Wall, S.A., Chrzanowska, K.H., Maxson Jr., R.E., 2000. Functional haploinsufficiency of the human homeobox gene MSX2 causes defects in skull ossification. Nat. Genet. 24, 387–390.
Yeo, G.H., Cheah, F.S., Winkler, C., Jabs, E.W., Venkatesh, B., Chong, S.S., 2009. Phylogenetic and evolutionary relationships and developmental expression patterns of the zebrafish twist gene family. Dev. Genes. Evol. 219, 289–300.
Zhao, J., Bradfield, J.P., Li, M., Zhang, H., Mentch, F.D., Wang, K., Sleiman, P.M., Kim, C. E., Glessner, J.T., Frackelton, E.C., Chiavacci, R.M., Berkowitz, R.I., Zemel, B.S., Hakonarson, H., Grant, S.F., 2011. BMD-associated variation at the Osterix locus is correlated with childhood obesity in females. Obesity 19, 1311–1314.